

Metal-to-insulator transition and magnetic ordering in $\text{CaRu}_{1-x}\text{Cu}_x\text{O}_3$

I. M. Bradarić,^{a, *} I. Felner^b and M. Gospodinov^c

^a *Laboratory for Theoretical and Condensed Matter Physics, The "Vinča" Institute of Nuclear Sciences
P.O. Box 522, 11001 Belgrade, Serbia, Yugoslavia.*

^b *The Racah Institute of Physics, The Hebrew University of Jerusalem,
Jerusalem 91904, Israel.*

^c *Bulgarian Academy of Sciences, Institute of Solid State Physics,
72 Tzarigradsko Chaussee Boulevard, Sofia 1784, Bulgaria.*

(October 25, 2018)

CaRuO_3 is perovskite with an orthorhombic distortion and is believed to be close to magnetic ordering. Magnetic studies of single crystal and polycrystalline $\text{CaRu}_{1-x}\text{Cu}_x\text{O}_3$ ($0 \leq x \leq 15$ at.% Cu) reveal that spin-glass-like transition develops for $x \leq 7$ at.% Cu and obtained value for effective magnetic moment $p_{\text{eff}} = 3.55 \mu_B$ for $x = 5$ at.% Cu, single crystal, indicates presence of Ru^{5+} . At higher Cu concentrations more complex magnetic behaviors are observed. Electrical resistivity measured on polycrystalline samples shows metal-to-insulator transition (MIT) at 51 K for only 2 at.% Cu. Charge compensation, which is assumed to be present upon $\text{Cu}^{2+/3+}$ substitution, induces appearance of Ru^{5+} and/or creation of oxygen vacancies in crystal structure. Since the observed changes in physical properties are completely attributable to the charge compensation, they *cannot be related* to behaviors of pure compound where no such mechanism is present. This study provides the criterion for “good” chemical probes for studying Ru-based perovskites.

PACS Numbers: 71.30.+h, 75.30.Hx, 75.30.Kz, 75.50.Lk

I. INTRODUCTION

Following the discovery of superconductivity in Sr_2RuO_4 at $\approx 1 \text{ K}^1$ the wide interest in Ru-based perovskites has been generated, due to diversity of unusual physical properties discovered. Structurally related Ca_2RuO_4 , which has the same crystal structure as high T_c superconductor $\text{La}_{2-x}\text{Sr}_x\text{CuO}_4$, is nonmetallic and shows antiferromagnetic (AFM) ground state below $T_N = 110 \text{ K}^{2-4}$. On the other hand SrRuO_3 and CaRuO_3 ($n = \infty$ members of the alkaline earth-ruthenium Ruddlesden-Popper⁵ series $(\text{Sr,Ca})_{n+1}\text{Ru}_n\text{O}_{3n+1}$) are exceptionally interesting *per se*. Both compounds adopt the same perovskite structure with an orthorhombic distortion (GdFeO₃ structure type) and are metallic conductors. SrRuO_3 is the only known ferromagnetic (FM) conductor among the $4d$ oxides (Curie temperature $T_c = 165 \text{ K}$), whereas CaRuO_3 has been recently shown to have spin-glass-like magnetic ground state.⁶ Since a common structural feature of the two compounds is that they are composed of an array of corner-shared octahedra RuO_6 , it is assumed that the degree of tilting and rotation of these octahedra from ideal cubic-perovskite structure governs the observed differences in the magnetic ground states. A narrow itinerant $4d$ band is formed through hybridization of Ru t_{2g} and O $2p$ orbitals. The $4d$ bandwidth thus formed sensitively depends on degree of hybridization.⁷ One of powerful tools to study physical properties of such systems is realized through chemical substitution. Recent results on the effects of chemical substitutions in CaRuO_3 show following: $\text{Ca}_{0.95}\text{Na}_{0.05}\text{RuO}_3$ ⁸ spin-glass or AFM ordering at 55 K, $\text{CaRu}_{1-x}\text{Sn}_x\text{O}_3$ ⁹ spin-glass ordering for $4 \leq x \leq 10$ at.% Sn and MIT for $x \geq 16$ at.% Sn and $\text{CaRu}_{1-x}\text{Rh}_x\text{O}_3$ ¹⁰ magnetic ordering (spin-glass?) for all x and MIT for $x \geq 7$ at.% Rh. From these studies it is evident that physical properties of CaRuO_3 are much more influenced by Rh than Sn substitution. Substitution of nonmagnetic Sn^{4+} for Ru^{4+} represents only lattice frustration and magnetic dilution of Ru-sublattice. On the other hand, Rh^{4+} ($4d^5: t_{2g}^5 e_g^0$) with $S = 1/2$ in the low-spin state, behaves as magnetic impurity, since it substitutes Ru^{4+} ($4d^4: t_{2g}^4 e_g^0$) with low-spin $S = 1$. Nevertheless, it is likely that Rh assumes valence state Rh^{3+} ($4d^6: t_{2g}^6 e_g^0$), $S = 0$, when incorporated in Ru-sublattice and thus produces charge frustration of the system. In order to clarify this issue,

*Corresponding author. Fax: +381 11 3440 100, e-mail: bradadic@rt270.vin.bg.ac.yu

we have chosen $\text{Cu}^{2+}(3d^9)$, $S = 1/2$, as substitution for Ru^{4+} , since this inevitably represents both charge and spin frustration. CaCuO_2 is considered as the parent of the cuprate family of superconducting compounds, consisting of CuO_2 sheets with AFM ordering of Cu^{2+} neighboring cations. Although CaRuO_3 and CaCuO_2 are not isostructural, we have assumed that appreciable amount of Cu can be incorporated in Ru-sublattice, while preserving the crystal structure. Furthermore, recent discovery of coexistence of magnetism and superconductivity in ruthenium-based layered cuprates $\text{Ln}_{1.4}\text{Ce}_{0.6}\text{RuSr}_2\text{Cu}_2\text{O}_{10-\delta}$ and $\text{LnRuSr}_2\text{Cu}_2\text{O}_8$ ($\text{Ln}=\text{Eu, Gd}$)^{11–14} proves an added motivation for this study.

In this paper we report results of magnetic and electrical resistivity properties of $\text{CaRu}_{1-x}\text{Cu}_x\text{O}_3$ ($0 \leq x \leq 15$ at.% Cu). We show here that Cu substitution on Ru sites profoundly alters ground state properties of CaRuO_3 introducing mixed oxidation states of Ru cations.

II. EXPERIMENTAL DETAILS

Polycrystalline samples of $\text{CaRu}_{1-x}\text{Cu}_x\text{O}_3$ ($0 \leq x \leq 15$ at.% Cu) were prepared by solid-state reaction from the appropriate stoichiometric mixtures of Ru metal powder, CaCO_3 and CuO (purchased from Strem Chemicals Inc.). The samples were mixed, ground and preheated at 850°C for 24 h in air. The powders were then reground, pressed into pellets and heated at $1000 - 1200^\circ\text{C}$ for 72 h in air, with two intermediate grindings. Single crystals of $\text{CaRu}_{1-x}\text{Cu}_x\text{O}_3$ ($x = 0, 5, 10$ and 15 at.% Cu) were grown from ground mixture of sintered samples and CaCl_2 flux in the ratio 1:30 (sample : flux). The mixture was heated to 1260°C and soaked at this temperature for 24 h, followed by slow cooling at a rate 2°C/h to 1000°C and finally quenched to room temperature to avoid possible twinning. The crystals tend to form in almost square planar shape with sizes around $0.4 \times 0.4 \times 0.02\text{mm}^3$, with short dimension along c -axis. The single crystals and sintered polycrystalline samples were characterized by energy dispersive x-ray analysis (EDAX), scanning electron microscopy (SEM) and powder x-ray diffraction (XRD) measurements. Powder x-ray diffraction measurements were performed on a Philips 1010 powder diffractometer using $\text{Cu K}\alpha$ radiation at room temperature. DC magnetic measurements were performed by a Quantum Design superconducting quantum interference device (SQUID) magnetometer. Resistivity measurements were performed on polycrystalline samples employing standard four-point method. Unfortunately, due to extreme fragility of single crystals, several attempts to measure resistivity were not successful.

III. RESULTS AND DISCUSSION

The samples are of single phase and crystallize in perovskite structural type with orthorhombic structure, space group $Pnma$ (62). Our results for the lattice parameters of single crystal and polycrystalline samples are in excellent agreement with values previously published.^{15,16} At concentrations greater than 15 at.% Cu, small impurity diffraction lines of CuO appear so that it is assumed that at this concentration the solubility limit is reached. The concentration dependence of the room temperature lattice parameters and the volume of the unit cell for polycrystalline samples are shown in Fig. 1. The data for a and b axes show the expected Vegard's law linear expansion assuming that larger Cu^{2+} (ionic radius 0.73 \AA) substitutes Ru^{4+} (ionic radius 0.62 \AA). On the other hand, c -axis is almost constant below 2 at.% Cu and then shows a linear shrinkage with increasing Cu concentration. Similar behavior has been observed in $\text{La}_{2-x}\text{Sr}_x\text{Cu}_{1-y}\text{Ru}_y\text{O}_{4-\delta}$ ^{17,18} for $x = 2$ and $0.7 \leq y \leq 1.0$. Nevertheless, the volume of the unit cell increases with x , as expected.

Shown in Fig. 2 is the magnetization vs temperature for $\text{CaRu}_{0.95}\text{Cu}_{0.05}\text{O}_3$ single crystal measured at various values of magnetic field applied along $[001]$ direction, under field-cooled (FC) and zero-field-cooled (ZFC) conditions. An irreversibility phenomenon associated with spin-glass-like behavior in CaRuO_3 (see inset of Fig. 2) is clearly present in this case. Note the strong field dependence of the irreversibility temperature T_{irr} (defined as the divergent point in the ZFC and FC curves). Furthermore, the broad peak around 35 K in the ZFC curve at 100 Oe is shifted to 29 K at 500 Oe and completely smeared at 1 kOe.

The observed spin-glass behavior can be accounted for by assuming the following simple model: Cu^{2+} and/or Cu^{3+} substitution for Ru^{4+} produces charge frustration of the system and therefore requires partial oxidation of neighboring Ru^{4+} cations to higher valence state Ru^{5+} ($4d^3$). This frustration is not local since the next-to-nearest-neighbors will also be affected, undergoing partial reduction to Ru^{3+} ($4d^5$). In this manner, charge compensation mechanism may

affect the valence state and therefore the magnetic moment of Ru cations at appreciable distance from Cu cation, simultaneously reducing the number of available conduction paths. According to Ref. 19, the signs of transfer integrals for 180° cation-anion-cation (CAC) superexchange interactions between octahedral-site cations are predicted to be ferromagnetic for all $\text{Cu}^{2+/3+}\text{-Ru}^{3+/4+/5+}$ combinations and antiferromagnetic for $\text{Cu}^{2+}\text{-Cu}^{2+}$, $\text{Ru}^{5+}\text{-Ru}^{3+}$ (weak), $\text{Ru}^{4+}\text{-Ru}^{3+}$ (weak) and $\text{Ru}^{5+}\text{-Ru}^{5+}$ combinations. Therefore, mixed interactions together with random distribution of Cu atoms within Ru-sublattice create necessary ingredients for spin-glass ordering. Within the framework of the proposed scenario, ferromagnetic clusters are formed around Cu impurities with AFM interactions within and between clusters, introducing frustration that result in a spin-glass behavior.

We fitted the data of $\chi(T) = M(T)/H$ (single crystal) in the paramagnetic range ($120 \leq T \leq 250$ K) to the modified Curie-Weiss (CW) law $\chi(T) = \chi_0 + C/(T - \theta)$, where χ_0 is the temperature independent term, C is the Curie constant and θ is the CW temperature. The value of the effective magnetic moment (deduced from the Curie constant C) $p_{\text{eff}} = 3.55 \mu_B$ is remarkably close to the expected Hund's rule value $3.87 \mu_B$ for Ru^{5+} with $S = 3/2$ and $g = 2$, indicating presence of Ru^{5+} in this mixed-valent system. This is in marked contrast to $p_{\text{eff}} = 2.33 \mu_B$ obtained for CaRuO_3 single crystal,⁶ appropriate to $2.83 \mu_B$ expected for low-spin state ($S = 1$) Ru^{4+} . The Curie-Weiss temperature θ also drastically changes from $-36(1)$ K for CaRuO_3 to $-134(3)$ K for $\text{CaRu}_{0.95}\text{Cu}_{0.05}\text{O}_3$, showing enhanced AFM interactions. Furthermore, χ_0 a measure of the density of states near the Fermi surface drops from $\chi_0 = 9.5 \times 10^{-3}$ emu/mole Oe at $x = 0$ to $\chi_0 = 7 \times 10^{-4}$ emu/mole Oe at $x = 0.05$. This is consistent with resistivity behavior measured on polycrystalline samples shown in Fig. 7, where the onset of MIT is observed at 51 K and 69 K for $x = 0.02$ and $x = 0.05$ Cu concentrations, respectively.

Although these results support the charge compensation mechanism outlined above, yet another possibility for charge compensation realized by oxygen loss, i.e. creation of oxygen vacancies, can be significant. It has been shown for $\text{La}_{2-x}\text{Sr}_x\text{Cu}_{1-y}\text{Ru}_y\text{O}_{4-\delta}$,¹⁸ with K_2NiF_4 -type structure, that the oxygen vacancies are located exclusively in the vicinity of Cu cations, which consequently means local character of charge compensation. However, we believe that oxygen loss is not significant in our samples for $x \leq 7$ at.% Cu, since the lower concentration of Ru^{5+} , due to presence of oxygen vacancies, would increase conductivity and shift MIT to higher Cu concentrations, simultaneously reducing the MIT temperature for fixed x . Indeed, resistivity measurements (not shown here) performed on slightly reduced polycrystalline samples (annealed at 350° C in N_2 atmosphere for an hour) show metallic behavior in the measured temperature range $7 \leq T \leq 300$ K for $x \leq 3$ at.% Cu and decrease of MIT temperature from 87 K to 30 K for $x = 7$ at.% Cu.

Magnetic isotherms $M(H)$ at $T = 5$ K obtained after cooling in zero applied field for an almost square planar shaped $\text{CaRu}_{0.95}\text{Cu}_{0.05}\text{O}_3$ single crystal and polycrystalline samples are shown in Fig. 3. With increasing applied field along c -axis, $M(H)$ reaches saturation for $H \geq 2$ T, yielding very low saturation moment $p_0 = 0.044 \mu_B$. On the other hand, $M(H)$ for field applied perpendicular to c -axis (i.e. in plane), shows no sign of saturation up to $H = 5$ T. This behavior is markedly different from the anisotropy of the magnetization found in single crystal CaRuO_3 ,⁶ where the easy axis of magnetization along c -axis is determined. Isothermal magnetization obtained for polycrystalline $\text{CaRu}_{0.95}\text{Cu}_{0.05}\text{O}_3$ sample shows linear behavior with no qualitative difference from that obtained for polycrystalline CaRuO_3 . Small hysteresis loops at $T = 5$ K (not shown here) with essentially same coercive field of $H_c \approx 100$ Oe for both polycrystalline and single crystal samples are observed.

The temperature dependence of the magnetic susceptibility for polycrystalline (a) and $M(T)$ for single crystal (b) $\text{CaRu}_{0.9}\text{Cu}_{0.1}\text{O}_3$ are shown in Fig. 4. Apart from different irreversibility temperatures T_{irr} , observed for polycrystalline and single crystal materials (also present for $x = 0$ and 5 at.% Cu), truly remarkable difference is manifested here both in shape of FC and ZFC curves and the onset of magnetic ordering at T_0 for polycrystalline sample, but without any magnetic anomaly present in single crystal in this temperature range. $\chi(T)$ data for polycrystalline $\text{CaRu}_{0.9}\text{Cu}_{0.1}\text{O}_3$ sample show $T_{\text{irr}} \approx 80$ K and well defined maximum in ZFC curve at $T_0 \approx 9.2$ K ($H = 14$ Oe), Fig. 4a. At $H = 1$ kOe, T_{irr} is completely suppressed being essentially equal to T_0 , which is slightly shifted to lower temperatures at this field. On the other hand, $M(T)$ data for single crystal $\text{CaRu}_{0.9}\text{Cu}_{0.1}\text{O}_3$ resemble re-entrant spin glass (RSG) behavior. Note the pronounced FM-like shape of FC curves and also difference between T_{irr} and the onset of FM-like behavior. T_{irr} is strongly field dependent, decreasing rapidly with increasing field.

The increase of Cu concentration promotes the growth of FM clusters tending to establish long-range FM order. However, this process is opposed by two effects: 1) The influence of short range AFM interactions within and between FM clusters may become more prominent in sintered polycrystalline sample with randomly oriented microcrystallites than in macroscopic single crystal, thereby leading to freezing of magnetic moments at low temperatures. Spin disorder at grain boundaries and surfaces has been extensively studied recently,²⁰⁻²³ including the size-dependent magnetic properties.²⁴ We believe that these effects are present in this case, specially because the material shows intrinsic spin-glass properties. 2) The decrease of the average distance between Cu cations with increasing concentration leads to increased concentration of Ru^{5+} cations and thus higher probability for $\text{Ru}^{5+}\text{-Ru}^{5+}$ AFM superexchange interactions. Formation of Cu-O-Cu pairs, triplets etc. and creation of oxygen vacancies at higher Cu concentrations add to complexity of magnetic properties. The former effect provides possible explanation for differences in magnetic properties

between polycrystalline and single crystal $\text{CaRu}_{0.9}\text{Cu}_{0.1}\text{O}_3$. The growth of FM clusters is almost unrestricted in single crystal, which is reflected in extremely large coercive field $H_c = 2.2\text{ T}$ (see Fig. 5a). Saturation moment $p_0 = 0.14\ \mu_B$ deduced from $M(H)$ curve is significantly higher than $p_0 = 0.044\ \mu_B$ obtained for $\text{CaRu}_{0.95}\text{Cu}_{0.05}\text{O}_3$. The extracted paramagnetic values in the range $120 \leq T \leq 250\text{ K}$ are: $\chi_0 = 3.6 \times 10^{-4}\text{ emu/mole Oe}$, $\theta = -219\text{ K}$ and $p_{\text{eff}} = 3.48\ \mu_B$.

The increase of Cu concentration from 5 to 10 at.% Cu also leads to profound changes in $\rho(T)$ behavior (see Fig. 7), showing sharp increase of the MIT temperature from 87 K to above 300 K for $x = 7$ and 10 at.% Cu, respectively.

Shown in Fig. 6 are the magnetic susceptibility $\chi(T)$ vs temperature dependence for polycrystalline (a) and $M(T)$ for single crystal (b), $\text{CaRu}_{0.85}\text{Cu}_{0.15}\text{O}_3$ samples. Both effects mentioned above should be considered in this case, since the low temperature magnetic anomaly at T_0 , associated with freezing of FM clusters, is present in polycrystalline and single crystal material. However, note the change of shape of FC curve for polycrystalline sample at $H = 1\text{ kOe}$ and also change of slope at T_0 , which are not seen in single crystal. The onset of FM-like behavior at 70-80 K (FC curves) is very close for both forms of material and is virtually field independent for single crystal. Moreover, T_{irr} is also approximately equal and decreases rapidly with increasing field in similar manner. The behavior of low temperature magnetic anomaly observed in ZFC curves vs magnetic field is very similar for both single crystal and polycrystalline samples and shows slight temperature decrease with increasing field, being completely washed out at $H > 7.5\text{ kOe}$ in single crystal.

Magnetic hysteresis loop measured on single crystal after ZFC (see Fig. 5b) is drastically smaller, $H_c = 40\text{ Oe}$, than that seen for $x = 10\text{ at.}\%$ Cu, while saturation moment $p_0 = 0.2\ \mu_B$ is somewhat larger, in accordance with differences in magnetic properties. Fitting of $\chi(T)$ to the CW law within $120 \leq T \leq 250\text{ K}$ range yields: $\theta = -33.9\text{ K}$, $p_{\text{eff}} = 2.24\ \mu_B$ and $\chi_0 = 4.8 \times 10^{-3}\text{ emu/mole Oe}$. The higher Cu concentration, inevitable presence of oxygen vacancies at these concentrations and the temperature range of fitting (vicinity of the magnetic transition at $\approx 80\text{ K}$) may account for the striking change of the extracted paramagnetic values compared with those obtained for $x = 5$ and 10 at.% Cu single crystals.

Shown in Fig. 7 are the electrical resistivity data vs temperature for polycrystalline $\text{CaRu}_{1-x}\text{Cu}_x\text{O}_3$ samples. Although there is a close temperature correspondence between changes of slope of $d(\ln \rho/d(1/T^4))$ vs. $1/T^4$ and T_{irr} (T_0) for low applied magnetic field M(T) data (polycrystalline samples), the plots for $\ln \rho$ vs. temperature to the $-\nu$ th power ($1 \leq \nu \leq 1/4$) do not show linear parts in any temperature regions for any ν values. Therefore, formulae for variable-range-hopping (VRH) resistivity do not match exactly with the resistivity data. This is not surprising, considering the large differences in magnetic properties between single crystal and polycrystalline samples due to grain boundaries.

More detailed research, employing precise control of oxygen stoichiometry and complementary experimental methods, would provide the basis for full characterization of the $\text{CaRu}_{1-x}\text{Cu}_x\text{O}_3$ system. However, the main result of this study shows that substitution of $\text{Cu}^{2+/3+}$ cation for Ru^{4+} changes the valence state of the latter to Ru^{5+} , thereby introducing drastic changes in both resistivity and magnetic properties of the parent compound. Keeping in mind the obvious differences, similarity in $\rho(T)$ and $\chi(T)$ behavior with $\text{CaRu}_{1-x}\text{Rh}_x\text{O}_3$ ¹⁰ is quite appealing. While the spin-glass-like behavior in $\text{CaRu}_{1-x}\text{Cu}_x\text{O}_3$ (for $x > 0$) can be understood, at least qualitatively, the origin of the spin-glass-like transition observed in pure CaRuO_3 (lacking the evident source of perturbation) must be more subtle in nature and is *not related* to the former. Therefore, we conclude that chemical probes, which potentially alter the valence state of Ru^{4+} in $(\text{Ca,Sr})\text{RuO}_3$, are not adequate tools for obtaining deeper insight in physical properties of the parent compound. In this sense nonmagnetic probe like Sn^{4+} can provide much more information. Discussion of this issue is beyond the scope of this article and will be published elsewhere.

IV. CONCLUSIONS

In summary, we have shown that substitution of $\text{Cu}^{2+/3+}$ for Ru^{4+} in $\text{CaRu}_{1-x}\text{Cu}_x\text{O}_3$ alters the oxidation state of the neighboring Ru cations to Ru^{5+} , leading to spin-glass-like behavior for lower Cu concentrations ($x \leq 7\text{ at.}\%$ Cu) and complex magnetic behaviors for $x \geq 10\text{ at.}\%$ Cu. Simultaneously, MIT is observed for only 2 at.% Cu at 51 K. Physical processes involved, while being interesting *per se* and possibly useful for understanding complexities of other materials like $\text{GdRuSr}_2\text{Cu}_2\text{O}_8$,¹⁴ have different origin and therefore cannot be related to physical properties of the parent compound CaRuO_3 .

ACKNOWLEDGMENTS

We are indebted to Dr. D. Rodić for help in XRD analysis. I. M. Bradarić gratefully acknowledges support from the "Abdus Salam" ICTP, Trieste, Italy. The work in Jerusalem was supported by the BSF (1999).

-
- ¹ Y. Maeno, H. Hashimoto, K. Yoshida, S. Nishizaki, T. Fujita, J. G. Bednorz and F. Lichtenberg, *Nature* **372**, 532 (1994).
- ² S. Nakatsuji, S. Ikeda and Y. Maeno, *J. Phys. Soc. Japan* **66**, 1868 (1997).
- ³ G. Cao, S. McCall, M. Shepard, J. E. Crow and R. P. Guertin, *Phys. Rev. B* **56**, R2916 (1997).
- ⁴ M. Braden, G. Andre, S. Nakatsuji and Y. Maeno, *Phys. Rev. B* **58**, 847 (1998).
- ⁵ S. N. Ruddlesden and P. Popper, *Acta Crystallogr.* **11**, 54 (1958).
- ⁶ I. Felner, I. Nowik, I. Bradarić and M. Gospodinov, *Phys. Rev. B* **62**, 11 332 (2000).
- ⁷ P. A. Cox, R. G. Egdell, J. B. Goodenough, A. A. Hamnett and C. C. Naish, *J. Phys. C: Solid State Phys.* **16**, 6221 (1983).
- ⁸ M. Shepard, G. Cao, S. McCall, F. Freibert and J. E. Crow, *J. Appl. Phys.* **79**, 4821 (1996).
- ⁹ G. Cao, S. McCall, J. Bolivar, M. Shepard, F. Freibert, P. Henning, J. E. Crow and T. Yuen, *Phys. Rev. B* **54**, 15 144 (1996).
- ¹⁰ G. Cao, F. Freibert and J. E. Crow, *J. Appl. Phys.* **81**, 3884 (1997).
- ¹¹ L. Bauernfeind, W. Widder and H. F. Braun, *Physica C*, **254**, 151 (1995).
- ¹² L. Bauernfeind, W. Widder and H. F. Braun, *J. Low Temp. Phys.* **105**, 1605 (1996).
- ¹³ I. Felner, U. Asaf, Y. Levi and O. Millo, *Phys. Rev. B* **55**, R3374 (1997).
- ¹⁴ J. W. Lynn, B. Keimer, C. Ulrich, C. Bernhard and J. L. Tallon, cond-mat/0001456 31 JAN 2000, and *Phys. Rev. B* **61**, R14 964 (2000).
- ¹⁵ H. Kobayashi, M. Nagata, R. Kanno and Y. Kawamoto, *Mater. Research Bull.* **29**, 1271 (1994).
- ¹⁶ G. Cao, S. McCall, M. Shepard and J. E. Crow, *Phys. Rev. B* **56**, 321 (1997).
- ¹⁷ S. Ebbinghaus and A. Reller, *Solid State Ionics* **101-103**, 1369 (1997).
- ¹⁸ S. Ebbinghaus, M. Fröba and A. Reller, *J. Phys. Chem. B* **101**, 9909 (1997).
- ¹⁹ J. B. Goodenough in *Magnetism and the Chemical Bond*, p. 174, (John Willey & Sons, 1966).
- ²⁰ N. Zhang, S. Zhang, W. P. Ding, W. Zhong and Y. W. Du, *Solid State Commun.* **107**, 417 (1998).
- ²¹ N. D. Mathur, G. Burnell, S. P. Isaac, T. J. Jackson, B. -S. Teo, J. L. MacManus-Driscoll, L. F. Cohen, J. E. Evetts and M. G. Blamire, *Nature* **387**, 266 (1997).
- ²² R. H. Kodama, A. E. Berkowitz, E. J. McNiff, Jr. and S. Foner, *Phys. Rev. Lett.* **77**, 394 (1996).
- ²³ B. Martinez, X. Obradors, Ll. Balcells, A. Rouanet and C. Monty, *Phys. Rev. Lett.* **80**, 181 (1998).
- ²⁴ J. P. Chen, C. M. Sorensen, K. J. Klabunde, G. C. Hadjipanayis, E. Devlin and A. Kostikas, *Phys. Rev. B* **54**, 9288 (1996).

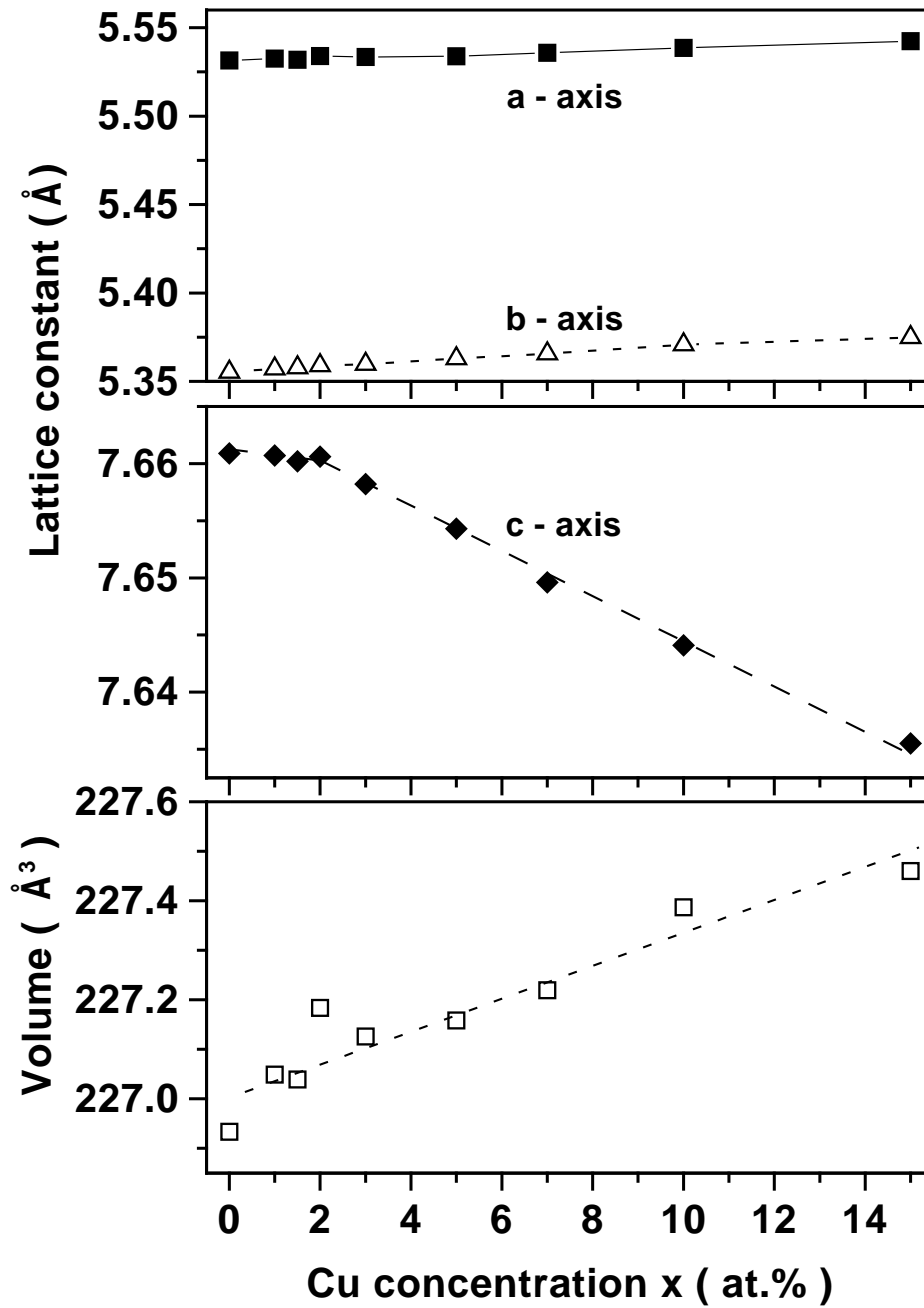


FIG. 1. Room temperature lattice parameters and the volume of the unit cell vs Cu concentration for polycrystalline $\text{CaRu}_{1-x}\text{Cu}_x\text{O}_3$.

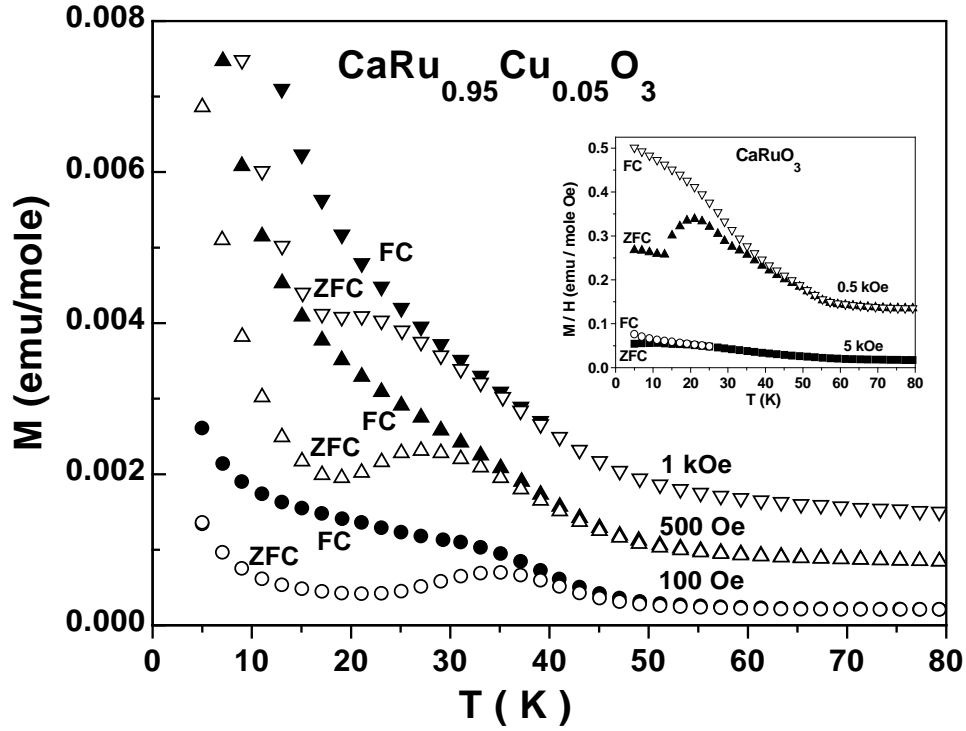


FIG. 2. $M(T)$ vs T (FC and ZFC) curves for $\text{CaRu}_{0.95}\text{Cu}_{0.05}\text{O}_3$ single crystal measured at different magnetic fields applied along c -axis. Inset: $\chi(T) = M(T)/H$ vs T for CaRuO_3 single crystal ($H \perp c$ -axis).⁶

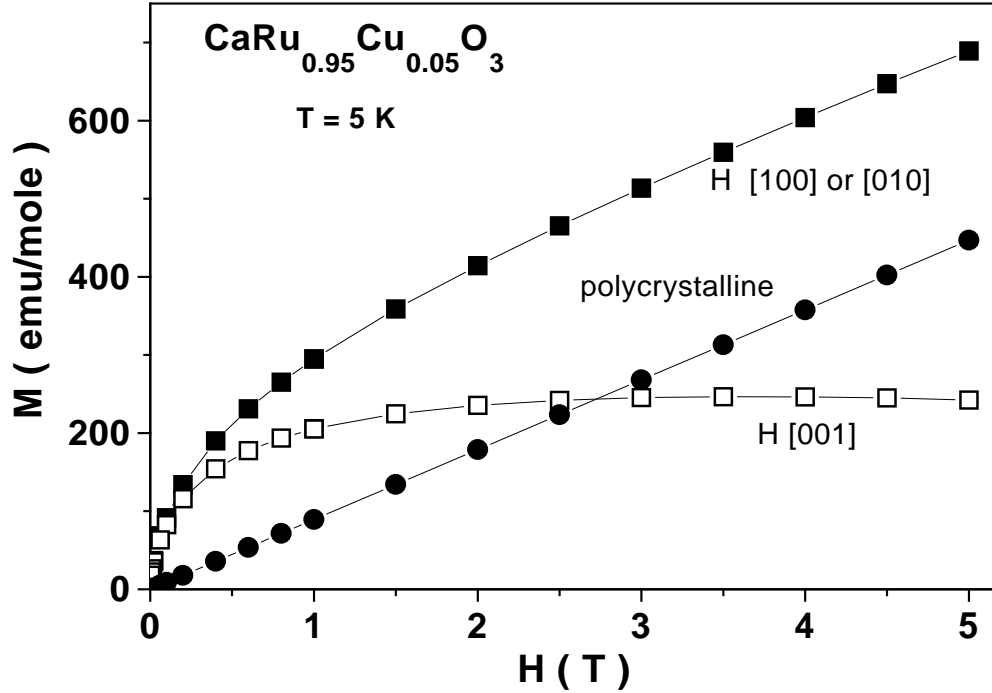


FIG. 3. Magnetic isotherms at $T = 5$ K for $x = 5$ at.% Cu single crystal and polycrystalline materials.

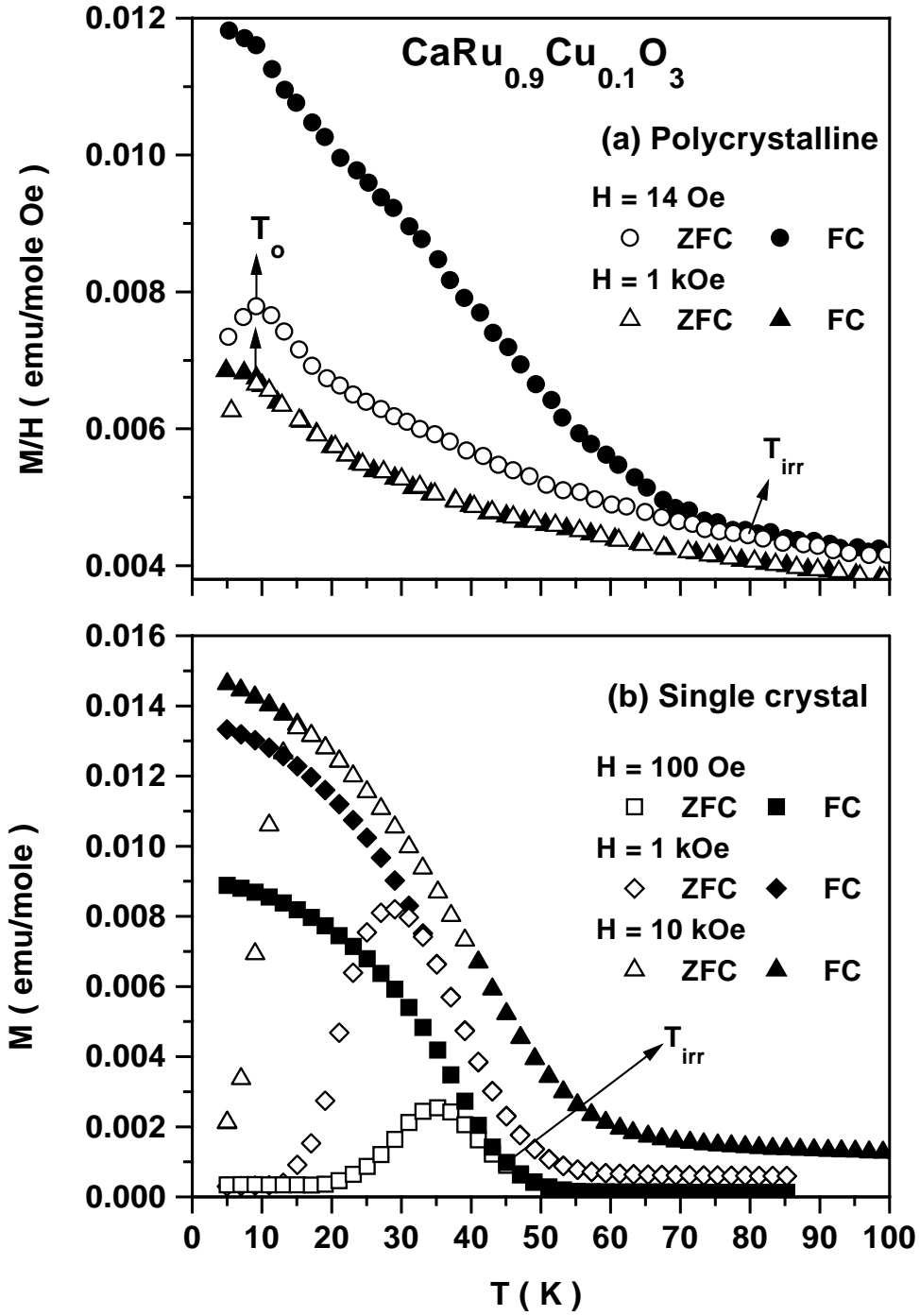


FIG. 4. FC and ZFC curves for $\text{CaRu}_{0.9}\text{Cu}_{0.1}\text{O}_3$ at different magnetic fields: (a) $\chi(T)$ vs T for polycrystalline sample and (b) $M(T)$ vs T for single crystal ($H \perp c$ -axis).

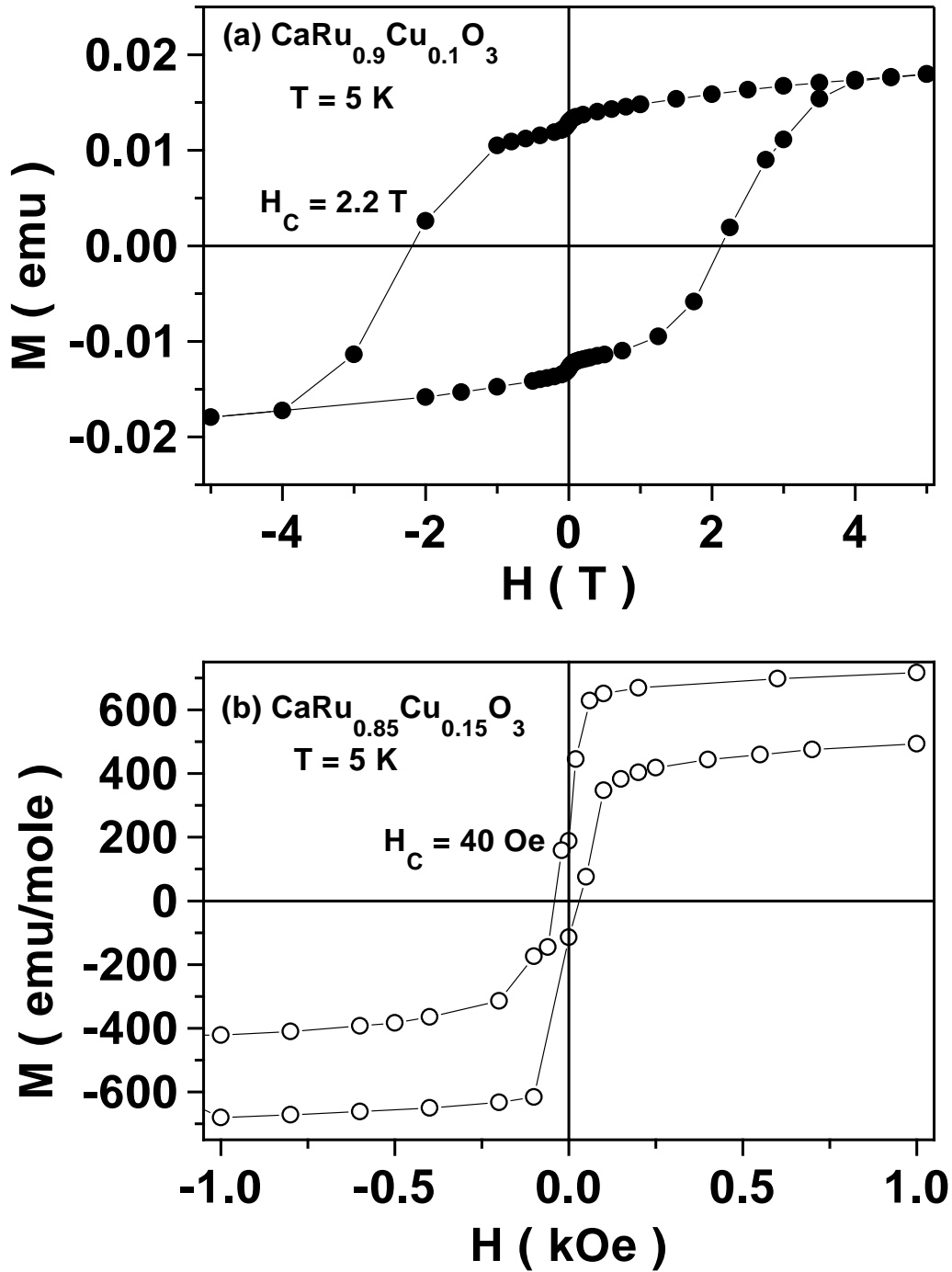


FIG. 5. Magnetic hysteresis loops at $T = 5 \text{ K}$ (ZFC) for single crystals: (a) $\text{CaRu}_{0.9}\text{Cu}_{0.1}\text{O}_3$ and (b) $\text{CaRu}_{0.85}\text{Cu}_{0.15}\text{O}_3$. Field is applied perpendicular to c -axis in both cases.

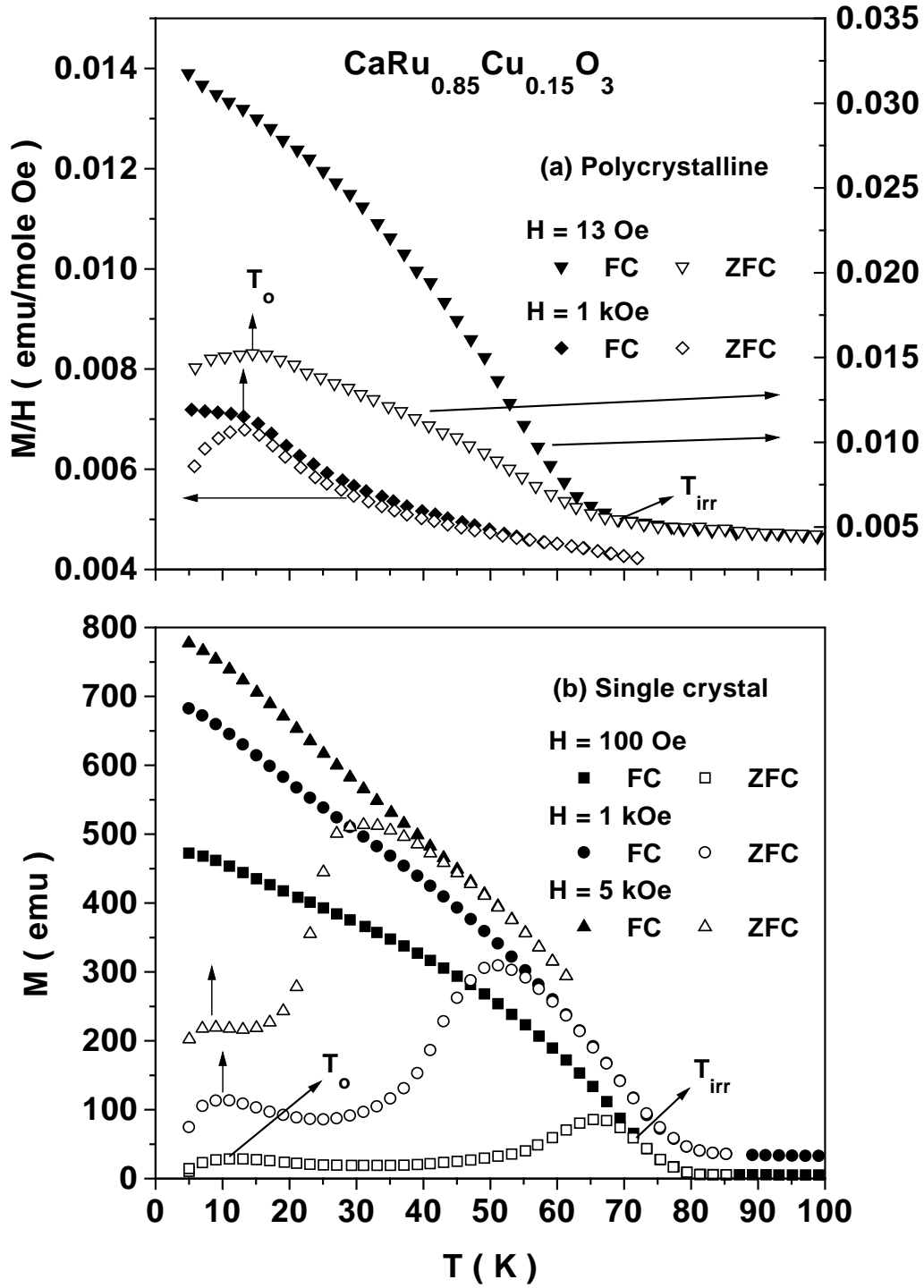


FIG. 6. FC and ZFC curves for $\text{CaRu}_{0.85}\text{Cu}_{0.15}\text{O}_3$ measured at different magnetic fields: (a) $\chi(T)$ vs T for polycrystalline sample and (b) $M(T)$ vs T for single crystal ($H \perp c$ -axis).

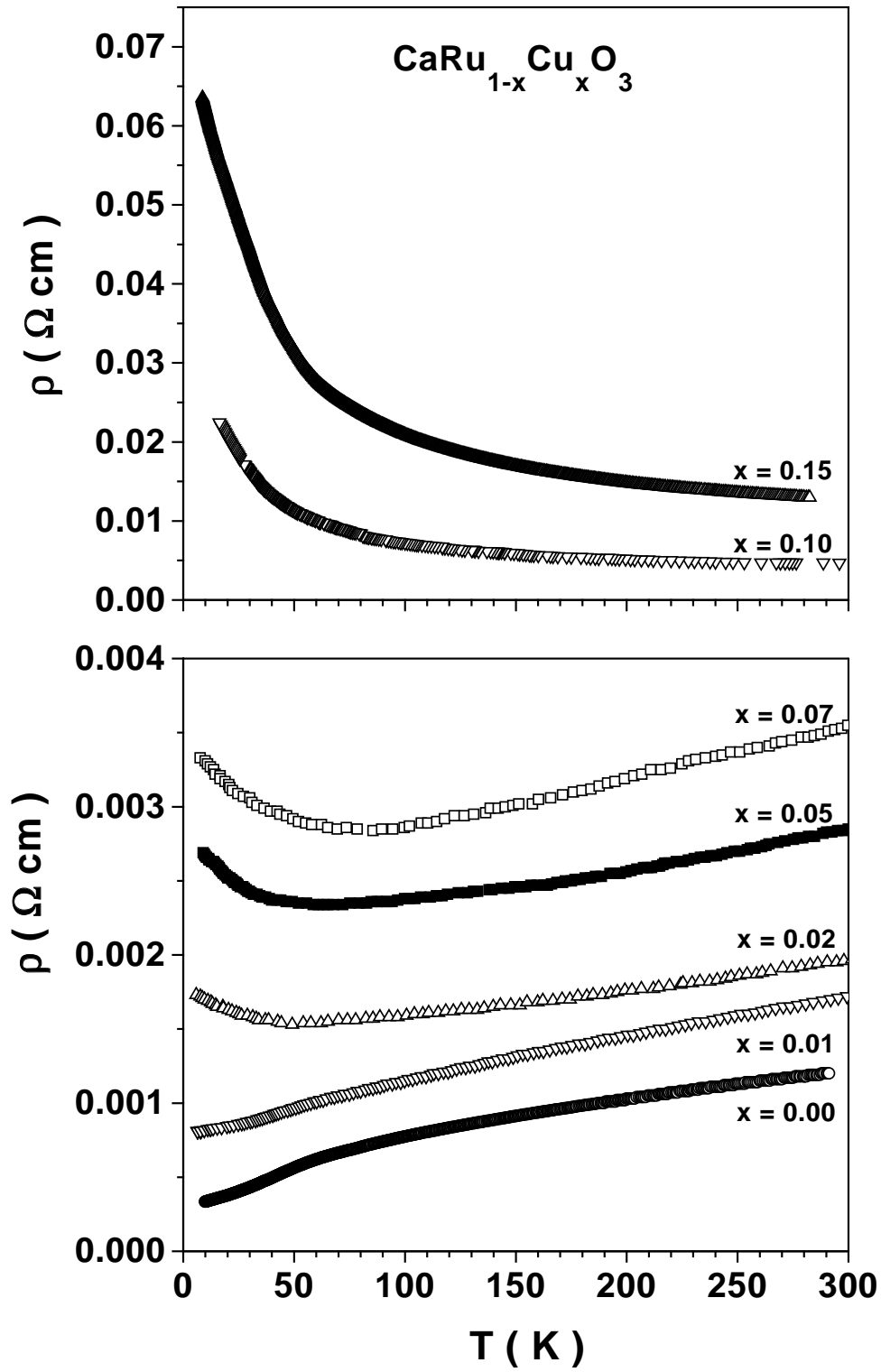


FIG. 7. Electrical resistivity $\rho(T)$ vs temperature T for polycrystalline $\text{CaRu}_{1-x}\text{Cu}_x\text{O}_3$ samples.